SSRG International Journal of Mechanical Engineering
ISSN: 2348-8360/ https://doi.org/10.14445/23488360/IJME-V13I7P103

Volume 13 Issue 7, 27-45, July 2026

Original Article

Simulation Study of Solar Flat Plate Collector Absorber Plate over the Primary Risers with Different Heights of External Radial Rectangular Fins

Vivek G[1], Lakshmipathy B[2], Ramesh P[3], Manivannan M[4]

[1,3]*Department of Mechanical Engineering, Annamalai University, Chidambaram, Tamil Nadu, India.*
[2]*Department of Mechanical Engineering, Annamalai University, Chidambaram, Tamil Nadu, India.*
[2]*Government Polytechnic College, Kadathur, Dharmapuri, Tamil Nadu, India.*
[4]*Department of Electronics & Instrumentation Engineering, Annamalai University, Chidambaram, Tamil Nadu, India.*

[1]*Corresponding Author : anandanvivek580@gmail.com*

Received: 01 April 2026 Revised: 30 May 2026 Accepted: 30 June 2026 Published: 30 July 2026

Abstract *- Solar water heaters are an established renewable-heat technology, although traditional flat-plate collectors suffer moderate thermal efficacies and heat losses, which may additionally be enhanced by operation and therefore encourage absorber-plate heat-transfer enhancement through geometric alterations, including fins. The aim of the numerical study was to isolate and quantify the effect of transverse fin height over the primary risers on the thermohydraulic performance to identify a suitable design that serves to optimize the useful heat gain without compromising on the acceptable hydraulic behaviour. A transient, pressure-based, finite-volume CFD model with conjugate heat transfer was simulated with automated, adaptive mesh refinement cut-cell meshing and grid-independence benchmarking on 3D absorber configurations (0, 5, 10, 15, and 20 mm fin height). A time-dependent temperature boundary of the top surface was considered to represent heating by the sun, and the remaining surfaces of the plates were maintained at 300 K; the simulations were done between 0-21,600 s (10:00-16:00). The increase in height of the fin increased normalized surface area in a monotonic way (40% at 0 mm and 100% at 20 mm; geometric enhancement of approximately 150%), whereas thermal performance was non-monotonic because of the fin-efficiency and conduction-resistance. The highest normalised efficiency is obtained on 15 mm fins (5% above the baseline), and maintaining Thermal efficiency About 38% During quasi study Time alongside (~13.1 kJ/kg of maximum specific exergy. 20 mm Fins minimized heat losses the most and have better temperature-field uniformity, but with diminishing returns and lower efficiency than 15 mm, in line with the decreasing fin effectiveness and increasing external losses. On the whole, the optimization in the absorber is dictated by thermogeometric considerations instead of surface-area considerations and 15 mm was found as the best fin height in the explored range to obtain maximum energy and exergy efficiency when operating under transient conditions.*

Keywords *- Absorber Plate, Cfd, Thermal Efficiency, Transverse Fins, Solar Water Heaters.*

1. Introduction

Solar Water Heaters (SWHs) are one of the most advanced and popular solar thermal technologies for domestic, commercial and industrial hot-water generation. The energy consumption for domestic hot water is a significant percentage of the total energy consumed in a building, from about 7.5% to 40%, depending on climatic and geographical conditions. Thus, solar water heating systems have become an environmentally friendly and economically viable alternative to the conventional fossil fuel-based water heating systems. Along with energy savings, SWHs play a significant role in renewable heat generation and in the global carbon-emission mitigation strategies [1]. A solar water heating system generally comprises a solar collector, thermal storage tank and circulation mechanism, either active or passive (thermosiphon) [2]. In passive systems, fluid circulation is caused by the density difference created by a temperature difference without the need for any external power supply [3]. The different collector technologies that are available are the most widely used Flat Plate Collectors (FPCs) and Evacuated Tube Collectors (ETCs). FPCs normally consist of a transparent glazing cover, absorber plate, riser tubes and thermal insulation, whereas the ETCs use vacuum insulation to reduce the convective and radiative heat loss and to get better thermal performance under low ambient temperature.

Even though the conventional solar collectors are technologically well-matured, they still suffer from thermal losses, moderate energy-conversion efficiencies, and solar irradiance fluctuations [4, 5]. The operational parameters, like infiltration of air, can be a major factor to increase the heat losses and thus the collector efficiency drops from 67.44% to 53.18%, and the overall heat-loss coefficient is affected [2, 6]. In the same way, the thermal efficiency can be decreased by up to 10% due to dust accumulation and improper collector orientation [3]. Therefore, it is important to investigate the improvement of absorber plate configuration and enhancement of the internal heat-transfer mechanism to maximize the solar collector performance.

The absorber plate is the most important energy-conversion part in a solar collector that absorbs incident solar radiation and then transfers it to the working fluid. It is determined by the thermal conductivity of its material, selective surface coatings, the thickness of plates and geometry. As well as improving the thermal efficiency, the changes in the absorber plate are also significant in controlling the temperature non-uniformity across the collector. High temperature differences may lead to the occurrence of hot spots, high thermal stresses, degradation of materials and negative effects on long-term system reliability. Hence, the optimization of the absorber plate should be done taking into account the three aspects: heat-transfer enhancement, temperature uniformity and thermal stability.

Some earlier works have been found to show that the performance of the collector can be enhanced substantially by making a few changes to the geometry of the absorber plate. For instance, step-modified absorbers have been reported with efficiency improvement from 4.6% to 12.7%, with the highest efficiency reaching 67.7% [7]. Of the different enhancement techniques studied, the use of transverse fins has become a subject of growing interest because it not only boosts the effective heat-transfer area but also enhances the thermal interaction between the absorber plate and the circulating fluid. The transverse fins can provide more pathways for conductive and convective heat transfer and disrupt the thermal boundary layers to facilitate the thermal response and enhance the overall heat-transfer rates [8].

Optimization of absorber plate geometry and enhancement of thermal transport in solar thermal collectors have been investigated using Computational Fluid Dynamics (CFD) for the last few years. Fin-assisted absorber configurations have been shown to improve the temperature uniformity, decrease thermal stratification and increase the useful heat gain due to better conductive heat spreading and convective heat transfer mechanisms [9]. Likewise, studies on other fin shapes have revealed that fin size plays a significant role in enhancing heat transfer and increasing hydraulic resistance, highlighting the need to consider the trade-off between thermal performance and pressure drop [10]. Additionally, transient CFD simulations showed that the outlet-fluid temperature and thermal effectiveness of the absorber plate could be significantly improved by modifying the absorber-plate design, underscoring the significance of thermohydraulic optimization in the design of collectors [11]. Further research on the fin height and fin spacing variations found that the temperature gradient, heat-transfer coefficient, and fluid-heating rate were significantly affected, and the fin geometry was one of the most important parameters that affect the collector performance [12]. Moreover, the results of the advanced CFD analysis showed that localized temperature non-uniformities can have a negative impact on both energy-collection efficiency and long-term reliability, and thus, fin dimensions need to be optimized to enhance the distribution of heat transfer while keeping the hydraulic characteristics acceptable [13]. All these results together validate the fin-assisted enhancement techniques and suggest that the independent effect of transverse fin height on the coupled thermal and hydraulic performance of SWH absorber plates is not yet well quantified.

Many enhancement methods have been suggested to enhance the thermal and thermohydraulic performance of solar thermal collectors. Geometric modification of absorber surface is still one of the most effective methods; sinusoidal absorber configuration has efficiencies of up to 25.29% [14], and V-corrugated zinc absorber has energy efficiencies of up to 49.96% [15]. Artificial roughening techniques such as gapped transverse ribs, trapezoidal ribs and honeycomb structure have shown significant improvement in heat transfer due to higher turbulence generation with thermohydraulic performance parameters as high as 2.12 and Nusselt numbers of more than 108 when the technique is operated at optimum conditions [16, 17]. Likewise, swirl-flow and insert-type enhancement methods have been shown to be very effective. The introduction of twisted-tape inserts in the ETCs resulted in thermal efficiencies around 30% higher than those of the conventional smooth-tube systems [18], and the use of coiled and curvilinear riser tubes for collectors yielded an improvement of about 30.03% in their performance due to the better disruption of the boundary layer and greater internal convection [19]. Fins and turbulators have been used in hybrid collector systems that have shown efficiencies as high as 79% over traditional flat-plate collectors. These enhancement techniques increase the performance of the heat transfer, but they can also cause an increase in hydraulic resistance and pressure-drop penalties. Therefore, the thermohydraulic optimization of a modern solar collector has become a more important focus of development, with thermohydraulic performance parameters becoming important characteristics to assess the overall performance of a solar collector.

Integrating energy storage and using intelligent optimization techniques are shown to be promising methods to enhance the solar thermal system performance. The use of Phase-Change Materials (PCMs) in the system can increase the thermal efficiency and maintain the outlet-fluid temperature by using the latent heat storage mechanism, which can improve the thermal availability for the periods of varying solar irradiance [20]. Moreover, according to the CFD-based investigations, it was observed that the outlet-water temperature was enhanced by about 7.3% when four fins were added as compared to unfinned cases, which showed the effectiveness of fin-assisted heat-transfer enhancement [8]. At the same time, optimization and Artificial Intelligence (AI) based approaches based on data have become more popular for solar thermal system design. The neural-network models coupled with particle swarm optimization and genetic algorithm have been able to predict with an accuracy of more than 99% in the application of finned solar air heater [21] and the Artificial Neural Network models have reduced the prediction error to less than ±5% for the thermal and exergy performances of solar air heater and also have saved much time for the optimization procedure as compared to the conventional CFD models [22]. All these are proof of the fact that the integration of thermal-energy-storage technologies, advanced numerical simulations, and intelligent optimization techniques for the design and operation of solar collectors is increasing.

The literature available as a whole shows that the performance of solar collectors can be significantly enhanced by means of geometric modifications, artificial roughness, turbulence promoters, PCM integration, and intelligent optimization techniques. However, the reported improvements are quite different due to the different collector setups, operating conditions and evaluation methods, and thus it is difficult to develop general design guidelines. Also, most of the investigations conducted so far are mainly on roughness elements, rib spacing, corrugated geometries, turbulence promoters, hybrid enhancement techniques and PCM-assisted collectors. The effect of transverse fin height on the temperature distribution of the absorber, transient thermal behaviour, useful heat gain, outlet fluid heating, pressure drop development and thermohydraulic performance have not been investigated systematically. Hence, the coupled nature of fin-height variation, temperature uniformity, thermal enhancement and hydraulic penalties is not well understood.

The novelty of the present work is that a systematic numerical study on the effect of fin height as an independent geometric design parameter of solar water heater absorber plates has been performed. The present study is different from the previous ones that have been conducted on generalized surface-enhancement techniques because it particularly assesses the effect of the fin height of the transverse fins on the heat-transfer characteristics, temperature distribution, pressure-drop behaviour, useful heat gain, thermal efficiency, and overall thermohydraulic performance under the same operating conditions. Hence, a detailed CFD simulation is conducted for the absorber plates with transverse fins of different heights to quantify their thermal and hydraulic performance and to determine an optimum fin-height configuration to improve the solar water heating applications.

2. Methodology and Geometry Configurations

The geometry of the absorber plate was created with the help of CAD tools and is ready to be preprocessed in CONVERGE. Critical structural dimensions were kept to guarantee the geometric fidelity, and features that are not necessary were simplified to minimize the computational cost without affecting the physical accuracy. The use of transverse fins was chosen over the traditional design of primary risers because it was determined that they would enhance the effective area of heat transfer and interfere with the development of hydrodynamic boundary layers along the risers. The resulting turbulence increases the convective heat transfer coefficient, and pressure penalties are controllable. The fin arrangement was added to an already optimized solar water heater design with secondary risers [23] in order to provide uniform fluid flow and isolate the direct effect of fin height on thermal enhancement.

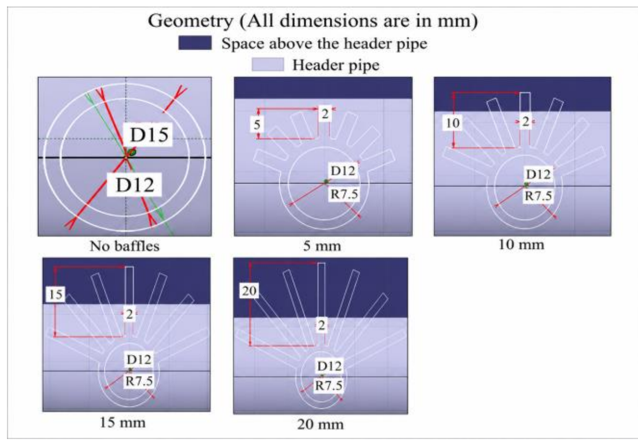

Fig. 1 Geometry configuration of the height of fins over the riser

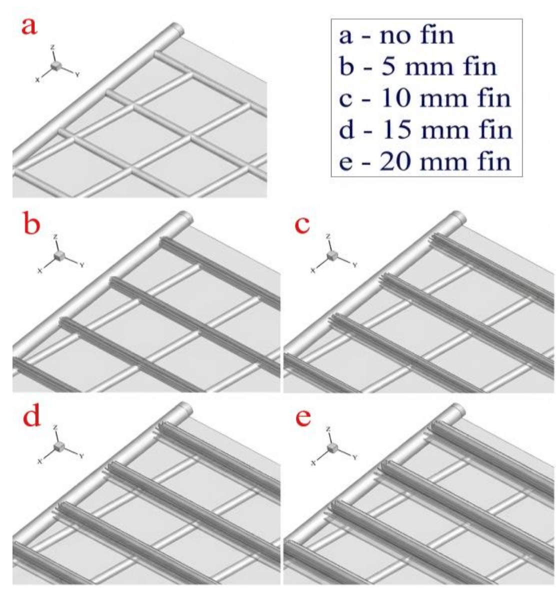

Fig. 2 3D geometry of the primary riser in absorber plate with, (a) no Fins, (b) 5 mm height fins, (c) 10 mm height fins, (d) 15 mm height fins, (e) 20 mm height fins.

A total of five configurations were produced in 3D format, with a difference in transverse fin height only, i.e. 0 mm (baseline), 5 mm, 10 mm, 15 mm and 20 mm as indicated in Figure 1. Geometric dimensions were all defined first in millimeters, and the space around the header pipe was kept constant to provide hydraulic consistency and allow parametric comparison to be controlled.

The height of the incremental fins can be systematically assessed in terms of surface area enhancement, enhancement of the turbulence, and possible trade-offs in the resistance of the flow.

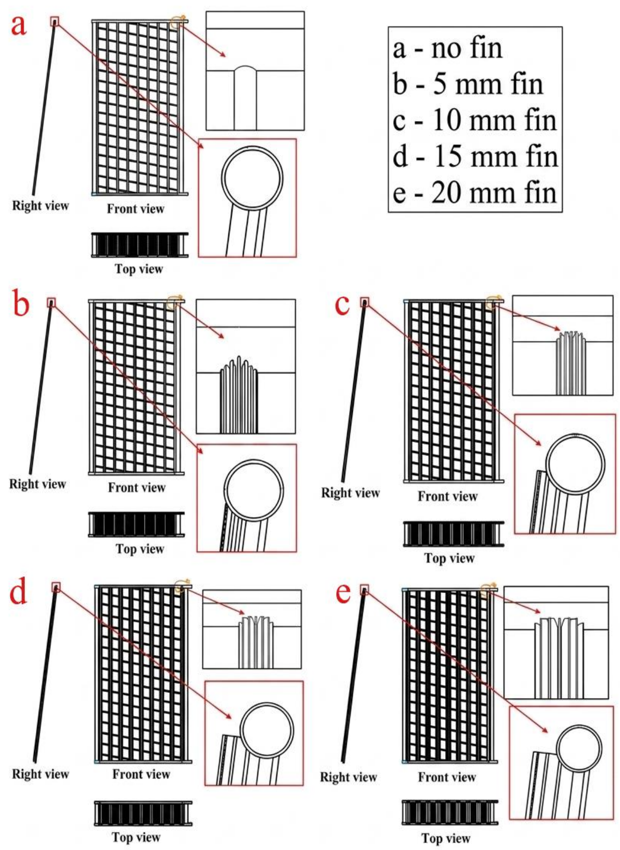

Fig. 3 primary risers with longitudinal fins projection of, (a) no fins, (b) 5 mm height fins, (c) 10 mm height fins, (d) 15 mm height fins, (e) 20 mm height fins.

The CAD tools that could be compatible with CONVERGE were used to construct the three-dimensional geometries so that the surface could be defined accurately to be used in CFD simulations. Figure 2 (a) to (e) shows the full 3D absorber plate models of each fin height.

Figure 3 (a) to (e) give projection and a magnified perspective to ensure the correct positioning of the fins and spatial positioning with the primary risers. These geometric verifications are necessary to guarantee that artificial disturbances of flow by misalignment are eliminated.

2.1. Computational Mesh Generation and Adaptive Mesh Refinement

The geometries were brought out in STL format and processed in CONVERGE Studio. In import, the geometry scaling was changed to metres so that when the Reynolds number and velocity scale were to be evaluated, and thermal gradients were to be assessed correctly, the scaling of the geometry was to be changed to millimeters.

The cut-cell Cartesian meshing strategy of CONVERGE was used to automatically create body-fitted meshes of complicated fin geometries. The regions of high temperature and velocity gradients were dynamically refined using Adaptive Mesh Refinement (AMR) in the vicinity of the absorber surface, transverse fins, and the fluid–solid interfaces. The cut-cell and AMR combination allowed for capturing the conjugate heat-transfer phenomena with accuracy and at the same time being efficient in computation.

To determine mesh independence, a grid independence study was conducted by continually refining the base grid size and AMR requirements until any change in the important thermal output parameters became insignificant.

2.2. Simulation Pre-Processing

2.2.1. Boundary Conditions

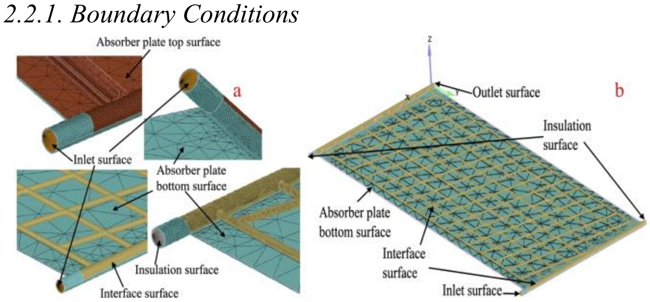

Fig. 4 (a) Boundary surfaces, (b) Boundary surfaces without absorber plate top portion.

The computational domain was described in CONVERGE Studio, which clearly distinguished fluid and solid domains to allow modelling conjugate heat transfer. The domain configuration (Figure 4 (a) & (b) was used to assign the location of the boundary surfaces, and visualization checks were done to verify that the surfaces were correctly labelled and that the domain was complete.

A time-dependent temperature boundary condition was prescribed to the absorber plate top surface by means of an external input file (Figure 5) and allowed one to simulate transient solar heating. The plate's bottom and lateral faces were kept at a uniform temperature of 300 K, which is the insulation and thermal conditions of the environment.

The walls were given zero normal gradients of both the temperature and the turbulence quantities, and the roughness of the wall was 0.5 as indicated in Table 1.

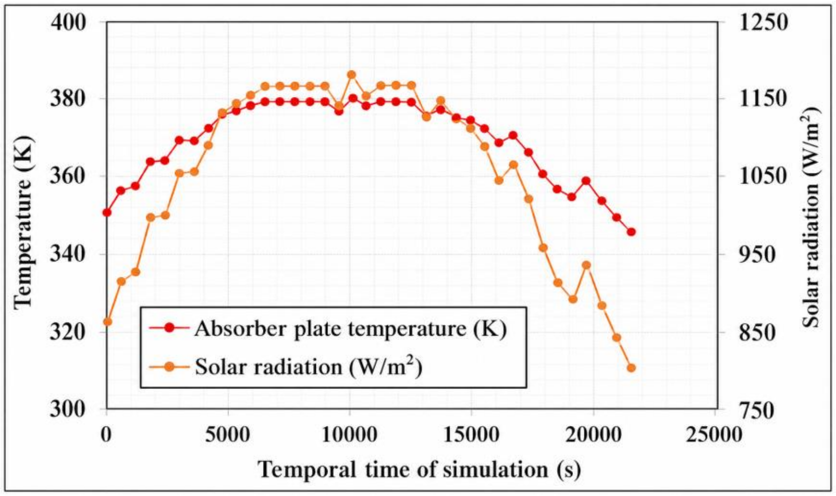

Fig. 5 Boundary condition of absorber plate assigned through the user file as temporal

Table 1. Initial and boundary conditions

Domain/ Surface	Type	Conditions
Domain initialization	Fluid	1. Temperature: 326 K 2. Pressure: 101325 Pa 3. Tke: 1.0 m2s2 4. Epsilon: 100 m2/s3 5. Species: H2O [Mass fraction is 1]
	Solid	1. Temperature: 351 K 2. Species: COPPER [Mass fraction is 1]
Absorber plate top surface	WALL	Temperature: Specified value (DI) through user file as shown in Figure 1.
Absorber plate bottom and side	WALL	Temperature [Specified value (DI)]:300 K
Insulation	WALL	1. Temperature: Zero normal gradient (NE) 2. Constant wall roughness: 0.5 3. Tke: Zero normal gradient (NE) 4. Epsilon: wall model
Surface between the fluid and solid domains	INTERFACE	Forward side: Fluid Reverse side: Solid
Inlet	INFLOW	1. Velocity [Mass flow]: 0.0066 kg/s 2. Temperature [Specified value (DI)]:307 K 3. Species [Specified value (DI)]: H2O [Mass fraction is 1] 4. Tke [Intensity]: 0.02 fraction 5. Epsilon [Length scale]:0.003m
Outlet	OUTFLOW	1. Pressure [Specified value (DI)]: 101325 Pa 2. Velocity: Zero normal gradient (NE)

2.2.2. Mesh Independence and Sensitivity Analysis

The base-grid size and the level of AMR were increased in a series of simulations to perform a mesh-independence study. The key performance parameters, such as absorber temperature, outlet-fluid temperature, useful heat gain, thermal efficiency and pressure drop, were monitored to ensure that the solutions were grid independent. The results obtained from the selected mesh did not show significant differences when further refinement was done, which verified the appropriateness of the selected mesh. Furthermore, the numerical sensitivity analysis showed that the thermal and hydraulic performance trends were consistent as the successive refinement levels were approached, and that the optimum configuration of 15 mm transverse-fin was not changed. These results validate the adopted CFD framework numerically in terms of stability and robustness. The monitored thermal and hydraulic performance parameters showed negligible differences with further mesh refinement, as the numerical discretization uncertainty was low and the adopted computational mesh was reliable.

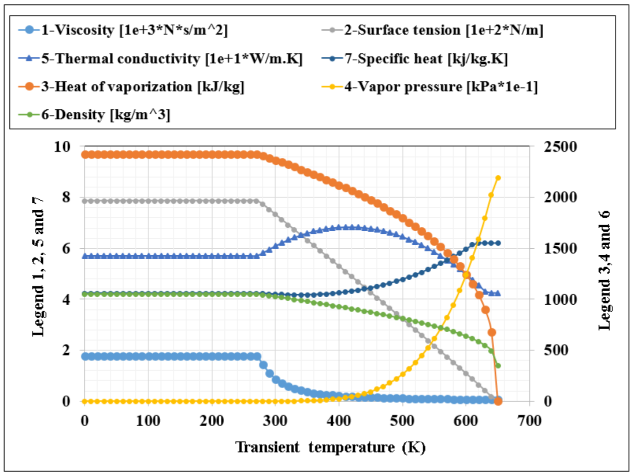

Fig. 6 Material properties assigned to fluid

2.2.3. Material Properties and Simulation Parameters

A working fluid was considered to be incompressible water (H_2O), and thermophysical properties were assigned as shown in Figure 6. The initial fluid state was established to be 326 K and atmospheric pressure (101,325 Pa), the turbulent kinetic energy was 1.0 $m^2/s^{2,}$ and the rate of turbulence dissipation was 100 m^2/s^3. The inlet boundary had a mass flow rate of 0.0066 kg/s with an inlet temperature of 307 K and turbulence intensity of 0.02, and a turbulence length scale of 0.003 m. The outlet boundary was taken to be a pressure outlet with zero normal gradient velocity of 101325 Pa to ensure that the flow developed as intended.

The absorber plate was assumed to be copper, the property of which was described in Table 2. At 351 K, the solid domain was started. Two-way thermal interaction between conduction in copper and convection in water was solved by the conjugate heat transfer coupling of the fluid-solid interface using CONVERGE.

Table 2. Properties of copper solid

Properties of copper	Values
Density [kg/m3]	8930
Specific heat [J/kg.K]	385
Thermal conductivity [W/m.K]	401
Melting point [K]	1700

Mass, momentum, and energy governing equations were solved with the transient pressure-based finite-volume formulation of CONVERGE. The pressure-velocity coupling was treated by an algorithm of implicit solution that was suitable in the case of incompressible flow. A higher-order scheme, which has a bounded scheme domain, was used to discretize convective fluxes to achieve numerical stability and reduce numerical diffusion. Iterative solvers that were equivalent to stabilized bi-conjugate gradient methods were used to solve linear systems to enable the system to converge robustly.

A pressure-based solver that is transient was used to solve the governing equations. The PISO algorithm was used to perform pressure-velocity coupling, and fluxes of convection were treated by a flux blending scheme, which allowed the use of a step limiter. The interpolation used in the Navier-Stokes equations was the Rhie-Chow legacy. The Successive Over-Relaxation (SOR) technique was used to solve momentum, density and energy equations, whereas the pressure equation was also solved with the HYPRE BICGSTAB solver.

The transient simulation was conducted between a time span of 0 to 21600 seconds (10:00 a.m. to 4:00 p.m.). Adaptive time stepping was limited to 1x10-5 s and 1.0 s to strike a balance between time resolution and computation time; the first-time step was set to 0.001 s. Numeral stability was achieved by keeping Courant Friedrichs Lewy (CFL) limits constant at 1.0 (Maximum convection limit), 2.0 (Maximum diffusion limit) and 50.0 (Maximum Mach limit), respectively.

Thermal and flow measurements were taken at pre-determined times to examine the dynamics of transient temperatures, heat transfer improvement and performance variability across each of the fin height configurations. Controlled geometric parameterization, automated cut-cell meshing and AMR, transient conjugate heat transfer simulation, and a clearly defined boundary condition give the framework of quantifying the effect of transverse fin height on the thermal performance of an absorber plate a numerically stable, physically consistent environment.

2.3. Model Validation and Limitations

The model's credibility was validated by comparing the results with those of published experimental studies of modified flat-plate solar collectors conducted by Himel et al. 2025 [7], which also showed that the same kind of modifications on the absorber surface led to higher outlet-fluid temperature, useful heat gain, and thermal efficiency. Further confidence is given by the fact that the authors have previously carried out CFD based on the same geometry, which showed a maximum deviation of only 0.167 K between the CFD results and the response-surface optimized results, showing excellent numerical consistency [23].

While the current study is only based on CFD simulation without any specific experimental measurements for the fin configurations studied, the validated simulation framework is a good basis to assess how the height of the transverse fins affects the thermohydraulic performance of the collector. Future studies should include experimental validation and analysis over a wider range of operating conditions to further increase the range of applicability of the proposed design methodology. The good agreement between the developed CFD framework and the experimental trends indicates the predictive reliability of the developed framework, which has been validated with previous experimental and numerical results.

3. Result and Discussion

3.1. Surface area and efficiency analysis

3.1.1. Surface area normalization and efficiencies

Figure 7 (a) shows the change of normalized surface area of the absorber and normalized thermal efficiency with transverse fin height (0-20 mm). Surface area grows monotonically with fin height, starting at about 40% with the unfinned setup, up to approximately 100% with 20 mm, which is a total geometric gain of approximately 150%. Normalized areas of 5, 10 and 15 mm yielded intermediate heights of 55% (37.5% increase), 70% (75% increase), and 85% (112.5% increase), respectively. This is also in line with the extended surface theory in the sense that the longer the fin height, the larger the effective absorber-fluid interface area and the larger the conductive heat spreading domain [24].

To the contrary, the normalized thermal efficiency has a non-monotonic behaviour. The efficiency with the baseline set is about 95% normalized. A 5 mm height cut efficiency to about 92% (3.2% efficiency reduction), and then increasing the height to 10 mm reduced it to about 88-90% (5-7% efficiency reduction). Although surface area is increasing, this is decreasing due to an augmented longitudinal conduction resistance and a diminution in the fin efficiency (η_f) with height leading to a decreased effective heat transfer per unit additional area [25].

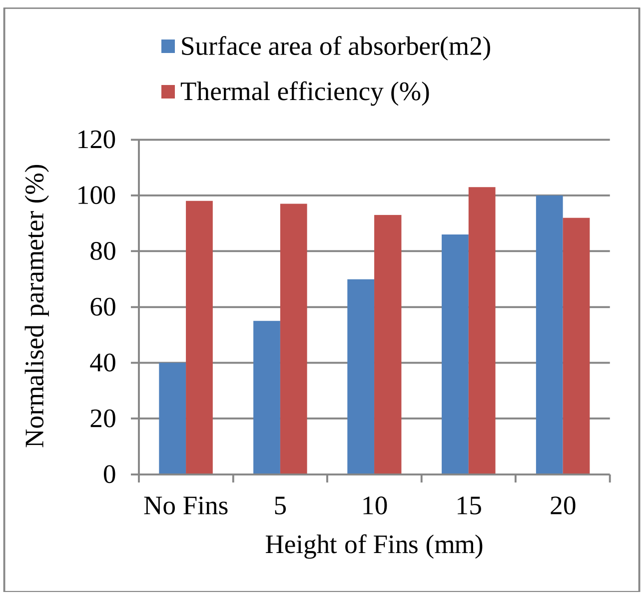

Fig. 7 (a) Normalization of surface area of different models and efficiencies

Throughout the cycle, the maximum thermal efficiency (15 mm) is achieved (approximately 100% normalization), and it is about 5% above the baseline. It means that this represents an optimal thermogeometric condition, in which surface area increase is compensated by conduction resistance without compromising fin effectiveness ($\boldsymbol{\varepsilon_f}$> 1) and convective heat loss.

Increasing fin height to 20 mm above this optimum increases normalized surface area to a level of 100% (17.6% In relation to 15 mm), but efficiency also decreases to ~90-92% (~8-10% Reduction from the peak). This deviation verifies the decreasing thermodynamic returns as a result of augmented conduction losses, augmented convective and radiative heat losses, and diminished fin efficiency as a result of larger temperature gradients on taller fins [26].

3.1.2. Temporal Variation in Thermal Efficiency

Figure 7 (b) depicts the temporary development of thermal efficiency of no fin, 5 mm, 10 mm, 15 mm and 20 mm transverse fin absorber configurations in 0-22,000 s. Three different regimes of response have been defined, namely, rapid transient rise, quasi-steady plateau, and late-stage decline, which is controlled by the dynamic equilibrium between useful heat gain, fin conduction behaviour and thermal losses.

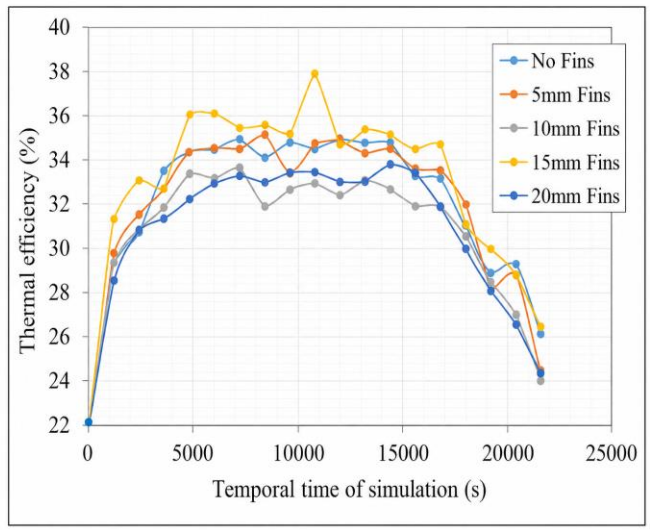

Fig. 7 (b) Temporal variation of thermal efficiency

The primary sharp rise in thermal efficiency is observed between 0-3000 s, when the thermal efficiency of all configurations is about 21-22% to 30-33%. Such a fast increase has been ascribed to the fact that the absorber is transiently charged thermally with low surface temperatures and low external losses [27]. In such circumstances, the energy balance as expressed in equation 1,

$$m_{abs}c_{abs}\frac{dT_s}{dt} = Q_{in} - Q_{loss} - Q_u \tag{1}$$

It is governed by useful heat gain because of high temperature differences between the absorber surface and the fluid. The 15 mm fin design has the quickest responding with a response of up to 33% within 3000 s due to the additional area of effective heat transfer and a low thermal inertia. Conversely, the 20 mm fins add more thermal weight and length of conduction path, slowing down the transient response by a small margin.

At the quasi-steady regime (~4000-17,000 s), effective heat transfer area and fin efficiency are the main determining factors of performance differences. The 15 mm setup remains efficient (34-38%), peaking at 38% of approximately 11,000 s.

The no-fin and 5 mm cases are within the range of about 33-35%, the 10 mm within the range of about 32-34% and the 20 mm within the range of about 31-33%, comparatively. The 15 mm fins will therefore be an average improvement of 2-3% points over the no-fin case and 3-5% points over the 20 mm one, which is a relative improvement of about 6-10% in steady operating conditions.

This high behaviour is attributed to the maximized effective heat transfer area (Equation 2),

$$A_{eff} = A_{base} + \eta_f A_f \quad (2)$$

where fin efficiency,

$$\eta_f = \frac{\tanh(mL)}{mL} \quad (3)$$

It is less when the conductive resistance increases with the height of the fin. In the case of 15 mm fins, conductive effectiveness and augmentation of the area are balanced. The advantage of extra geometric area is compensated by reduced fin efficiency and longer conduction path in the case of 20 mm. In addition, the exposure surface area increases convective and radiative losses, another restriction to the higher performance of taller fins.

All configurations begin to lose efficiency past the point of ~17,000 s, becoming converged at 22,000 s of 24-26%. In the case of the 15 mm fins, the decrease of the peak (~38%) to the final (~26%) is a decrease of 12% points (~31-32% relative reduction). This loss is connected with high temperatures of absorbers and nonlinear amplification of thermal losses, which leads to the fact that external dissipation mechanisms dominate over the effects of geometric enhancements. Consequently, the inter-configuration differences reduce in the late-stage regime [28].

3.1.3. Efficiency Improvement Strategies

Figure 7 (c) shows the percentage change in thermal efficiency versus transverse fin height (0, 5, 10, 15 and 20 mm). The findings show that there is no monotonic relationship between fin height and efficiency, showing that there is an optimal geometry configuration.

The 5 mm fin design has a slight decrease in efficiency (~ 1% less than the baseline) when compared to the No Fins. Significant efficiency loss is detected at 10 mm height, and it is about 5%. Comparatively, the height of the 15 mm fin produces the maximum efficiency increase of about +6%, with an increase to 20 mm producing a reduction of a factor of 4 (−5.5%). Therefore, the optimum change in net performance of the 15 mm fin height is approximately 11.5% better than the worst performance configuration (20 mm), which proves the occurrence of an optimal regime of interaction of heat transfer and flow at 15 mm.

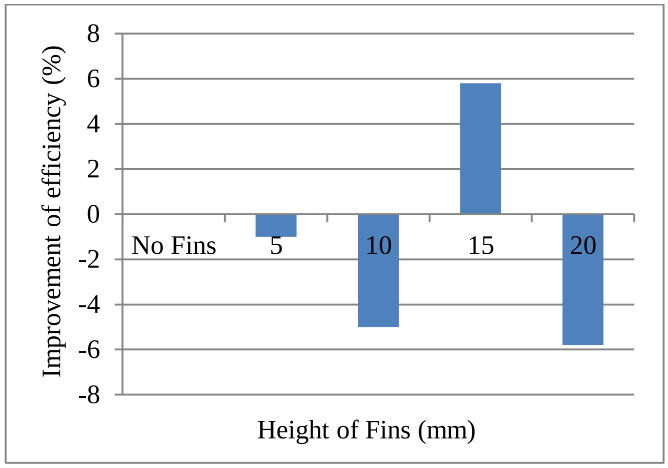

Fig. 7 (c) Efficiency improvement strategy from the base model

Thermodynamically, the efficiency difference that is observed is dictated by the trade-off between improved convective heat transfer and the hydraulic penalties. Fins cause an augmentation in the convective heat transfer, which is characterized by Equation 4:

$$Q_{conv} = hA_{eff}\left(T_s - T_f\right) \quad (4)$$

The hydraulic penalty of a higher fin height is calculated in the form of the Darcy-Weisbach (Equation 5):

$$\Delta P = f\frac{L}{D_h}\frac{\rho V^2}{2} \quad (5)$$

and the power of the pumping (Equation 6) of equal force will consume:

$$W_p = m\frac{\Delta P}{\rho} \quad (6)$$

The growth in effective surface area (A_{eff}) at 5 mm is too small to cause a significant increase in Q_u But slight increases in friction factor (f) and pressure drop (ΔP) counteract the thermal gains, causing a small decrease in efficiency.

At 10 mm, the increase in surface area continues, but in the process, the increase in fin Length (L) decreases the fin efficiency because the conduction resistance along the fin profile is increased. At the same time, impediments to the flow increase turbulence and dissipation of viscous energy, increasing (ΔP) and pumping power out of proportion [29]. This means that the hydraulic losses are not offset by the net useful heat gain and result in the observed reduction of efficiency by about 5%.

The 15 mm high of the fin is the trade-off thermo-hydraulic optimum. The increase in the coefficient of convective heat transfer (h) and effective area (A_{eff}) at this configuration is the largest and maximizes Q_u, with fin efficiency at an acceptable level. There is a high likelihood that the flow field will gain greater mixing without the generation of excessive recirculation areas or large-scale separation, which will moderate frictional losses. The optimum improvement in thermal efficiency (~6%) is a positive synergy of both amplified heat transfer and regulated pressure drop [30].

Nevertheless, the negative hydraulic effects prevail at 20 mm height. The higher the ratio of the fin, the higher the blockage and the more the boundary layer is disrupted, and the pressure drop (ΔP) is high. Also, the long fin length decreases fin efficiency because of the axial temperature gradient and high conduction resistance. The net decrease in the effective use of heat transfer and the pumping work results in a significant decrease in efficiency (~5.5%).

3.2. Heat loss and Temperature Analysis

3.2.1. Temporal Variation in Overall Heat Loss Rate

The time variation of the overall heat loss rate (Q_{loss}The baseline absorber and fin height of 5, 10, 15, and 20 mm is shown in Figure 8 (a). The response is typified by a short-term increase (0-3000 s), a quasi-steady plateau (3000-15000 s) and a gradual decrease after 15000 s. Fin integration in all regimes results in a sustained and systematic decrease in (Q_{loss}), and maximum mitigation of 37% in the 20 mm configuration compared to the baseline.

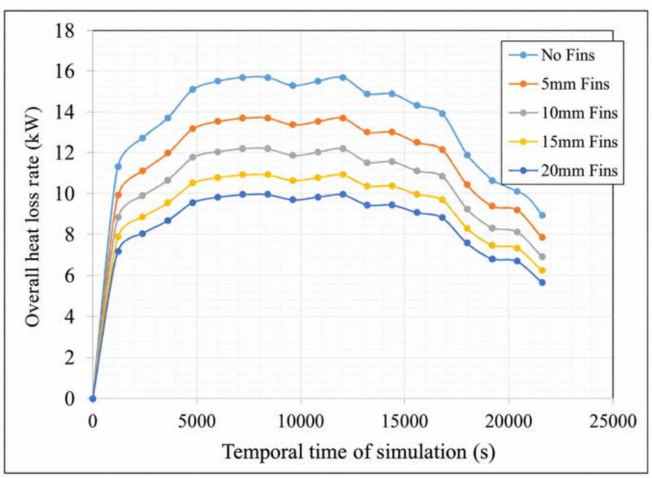

Fig. 8 (a) Temporal variation of overall heat loss rate

The baseline configuration increases to an approximate of 11.5 kW during the initial transient period, but 5, 10, 15, and 20 mm fins only increase to an approximate of 10.0, 9.0, 8.2 and 7.5 kW, respectively, representing a decrease of about 15, 22, 30 and 35%, respectively. Also, the decrease in convective loss is not only because of the diminished temperature difference but also because of the change in the convective coefficient. Therefore, temperature regulation via fin moderation of heat transfers inhibits direct and indirect (via diminished strength of buoyancy-induced convection) heat transfer in the same direction [31]. This combined inhibition is the cause of the severe inhibition in the initial stages, as seen in Figure 8 (a).

Maximum losses in the quasi-steady region (5000-12000 s) at the levels of the baseline, 5mm, 10mm, 15mm and 20mm are approximately 15.7 kW, 13.8 kW, 12.1 kW and 10.8 kW, respectively, which are proportional to the reduction of about 12, 23, 31 and 37%. In this regime, the system behaviour is given by Equation 7,

$$Q_{loss} = U_L A\left(T_p - T_\infty\right) \quad (7)$$

Although the area is increased, the overall heat loss coefficient (UL) at the fin height reduces with the height because of the redistribution of conductive fin. Increase in fin height increases conductive cross-sectional area (Ac), flattens temperature gradients, limits local thermal intensification, and decreases driving potential of external heat transfer. Also, the effective radiative heat transfer coefficient is negative with decreasing mean Temperature (Tm), which further decays radiative losses in the plateau region [32].

The difference between 15 mm and 20 mm fins (~5-6%), however, suggests the marginal improvement: geometric saturation, which is controlled by fin efficiency. The longer the fin height (L), the greater (mL) and the smaller ($\boldsymbol{\eta_f}$) and the more surface area can be used. As a result, at frequencies above 15 mm, the conduction benefit increment is partially compensated by a decreased fin efficiency, which is why the performance gain decreases.

During the late-stage decay (>15000 s), the heat loss drops to about 9.0 kW (baseline) and about 5.6 kW (20 mm) and is 30-38% lower than in configurations. The fin configurations reduce the initial thermal overshoot and hold a lower temperature potential during operation, hence sustaining lower levels of convective and radiative dissipation during the cooling process.

Collectively, the enhanced performance in Figure 8 (a) with growing fin height can be explained by the inhibition of absorber surface temperature, attenuation of radiative transfer that is nonlinear, reduction of buoyancy-driven convection by reduction of Grashof number, increased conductive heat spreading that reduces the effective overall heat loss coefficient and controlled fin efficiency by geometric saturation [32]. The 15 mm combination is almost optimally thermally moderated and 20 mm maximally reduced (approximately 37%) to prove fin height as a leading design factor determining temporal heat loss behaviour.

3.2.2. Thermal Efficiency–Fluid Temperature Difference Interaction

Figure 8 (b) shows that the thermal efficiency (η_{th}) is monotonically increasing as the fluid temperature difference increases in all fin configurations, where a clear performance order of 15 mm > 5 mm = 20 mm > 10 mm > no fins is observed in the investigated range of ~20 to 47 ℃. In a quantitative analysis, at ΔT = 20 ℃, $\boldsymbol{\eta_{th}}$ is about 21% with no fins to represent baseline (no fins) and 24-25% with 15 mm fins to represent an improvement of almost 15-18%.

With ΔT increasing to about 30 ℃, the efficiency increases to about 30 (no fins) and ~31-32% (15 mm), which represents a relative increase of 5-7. The 15 mm design reaches a high of about 37-38% at the greatest recorded ΔT (of the order of ~45-47 ℃), versus the 34-35% of the baseline, and an absolute difference of some 3-4% points (of the order of 9-11% relative improvement). The trend in improvement justifies that fin integration enhances heat transfer performance with high thermal driving potential.

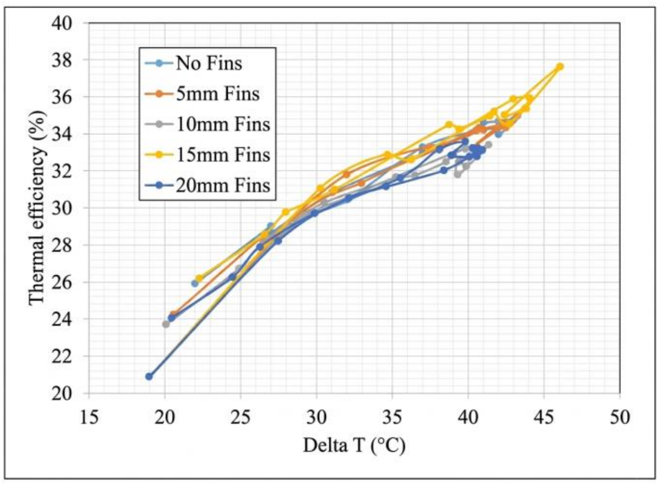

Fig. 8 (b) Thermal efficiency with fluid temperature difference

The resultant improvement can be strictly explained by the basic formulation of collector efficiency by the equation 8,

$$\eta_{th} = \frac{mc_p(T_{out} - T_{in})}{A_c G} \tag{8}$$

As mass flow rate, specific heat and incident solar flux are held constant at each configuration, the change in efficiency is directly proportional to ΔT. The improvement by the fin is, however, controlled by the increased rate of convective heat transfer (Equation 9):

$$Q_u = hA_{eff}(T_s - T_f) \tag{9}$$

When the fin height is raised, (A_{eff}) rises, hence, (Q_u) and therefore ΔT. The 15 mm fins have the best thermohydraulic synergy with the increase in (A_{eff}dominating the resistance to conduction and the penalty of flow disturbance. The relative performance of the 20 mm fins, which have a larger surface area, is relatively less, which means that there are diminishing returns dictated by fin efficiency.

With higher (L), (mL) rises, and it in turn reduces (η_f) because of the increasing conduction resistance with the fin length. Therefore, the marginal contribution of the heat transfer by the fin tip to the total heat transfer decreases, and this is why there was a slight decline in performance between 15 mm and 20 mm, even though the geometric area was larger [33].

Also, increased ΔT enhances the internal convective heat transfer coefficient due to augmentation by the Reynolds numbers effects due to mixing aided by buoyancy in the flow passages. The correlation of the Nusselt number suggests that fin height (15 mm) enhances (h), which increases energy extraction, when the flow turbulence is enhanced. Nevertheless, too high fin height (20 mm) probably increases the hydraulic resistance and stagnation regions, which leads to effective heat removal with the increased area.

Thus, Figure 8 (b) reaffirms the fact that an interdependent surface-area amplification and fin-efficiency optimization process controls thermal efficiency enhancement.

The 15 mm design is optimally thermal performing, with an optimum ratio of increased effective heat transfer area, favourable fin efficiency, and reduced conduction and hydrodynamic penalties leading to maximum performance of about 37-38% at ΔT – 47 ℃. This determines 15 mm to be the thermally optimal geometry in the studied geometries.

3.2.3. Absorber Temperature with Solid Temperature difference

Figure 8 (c) shows the dependence of the temperature of the absorber plate on the difference in absorber-solid temperature (ΔT) in the baseline (no fins) and fin-integrated configurations (5, 10, 15, and 20 mm). The no-fin design shows a monotonic decrease in absorber temperature between around 351 K at ΔT ≈ 0 °C up to almost 331 K at ΔT ≈ 28 °C with a moderate increase to about 342 K at ΔT ≈ 37 °C.

This initial value is a progressive conductive dissipation into the solid matrix and more vigorous convective extraction with increasing temperature gradient, according to the Fourier law of conduction, of more heat being lost to the solid with increasing temperature gradient [34]. The temperature recovery at higher ΔT is then seen to be indicating that the regime is where the heat input is greater than the rate of dissipation, which implies the beginning of the thermally stabilized energy storage between the absorber-solid system.

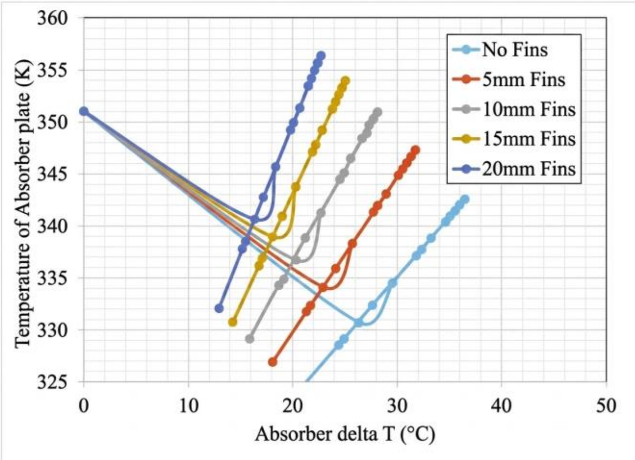

Fig. 8 (c) Temperature of the absorber with a difference in solid temperature

Under fin augmentation, the thermal characteristic is non-monotonic with a steady decrease at the beginning and a sharp increase in temperature at temperatures above ΔT ≈ 18–20 °C. In the case of 5 mm fins, the absorber temperature drops to a minimum of about 327 K at ΔT ≈ 18 °C and then increases continually, to about 347 K at ΔT ≈ 32 °C. The fin height of 10 mm will change the minimum temperature to approximately 329 K at ΔT ≈ 16 °C, and then increase to approximately 351 K at ΔT ≈ 29 °C. The 15 mm and 20 mm designs demonstrate a steadily increasing peak temperature of approximately at ΔT of 22-24 ℃ with a peak of about 354 K and 356 K, respectively. In quantitative terms, the 20 mm fins would increase absorber temperature by almost 22-23 K, or about 6-7% in absolute temperature level, which is an improvement of about 6-7% in the absolute temperature level. This is credited to the increased effective heat transfer surface and solid-absorber interaction that augments internal heat redistribution and, at the same time, minimizes localized thermal resistance [35].

The governing equation 10 of the absorber plate under steady-state conditions is as follows;

$$SA = hA\left(T_p - T_f\right) + U_L A\left(T_p - T_a\right) + \frac{T_p - T_s}{R_{cond}} \qquad (10)$$

The decrease in $Rcond$ caused by fin integration enhances the conductive heat exchange between the solid, and this changes the temperature distribution of the absorbers. In addition, the degree to which extended surfaces are efficient in heat transfer is dependent on fin efficiency. With increasing fin height (5 mm to 20 mm), the perimeter to area ratio gets better, so (mL) increases and therefore more capacity of heat dissipation is achieved, but enough absorber temperature is maintained because of better heat spreading.

The increase in absorber temperatures of the 15 mm and 20 mm fins at moderate ΔT is scientifically attributed to the increase in the lateral heat spreading, the decrease in thermal stratification and the increase in solid medium-absorber thermal storage synchronization. The enhanced conduction channel lowers the temperature gradient on the plate and hence, localized overheating is minimized, and the system can operate at increased mean absorber temperature without excessive loss [24]. Nevertheless, there is a possibility of diminishing returns owing to rising convective and radiative losses, which increase with absorber temperature. Figure 8 (c) shows quantitatively that, at 15-20 mm, fin augmentation maximises the conductive coupling and convective dissipation ratio to produce an absorber temperature increase of up to about 5-7% compared to the baseline, without any thermodynamic instability.

3.2.4. Solid and Fluid Temperature difference characteristics

Figure 8 (d) shows the simultaneous change in the mean fluid temperature difference (ΔTf) and the mean absorber (solid) temperature difference (ΔTs) of the base case of 5, 10, 15, and 20 mm fin heights. A strictly monotonic increase in ΔTs with ΔTf is seen in all configurations, though the slope $(\boldsymbol{\partial(\Delta T_s)/\partial(\Delta T_f)})$ progressively decreases with the fin height, which means more intensive convective heat transfer and less solid-fluid thermal disequilibrium. In the no-fin case, ΔTs rises considerably between 0℃ at ΔTf ≈ 20 ℃ and about 36-37 ℃ at ΔTf ≈ 42-43 ℃ with an average slope of about 1.6-1.7. This implies that the temperature of the absorber increases at a faster rate than that of the fluid, which means that the thermal resistance to convection on the surface is high, and that there is minimal convective heat loss [36]. Conversely, the 5 mm and 10 mm fin configurations have lower values of terminal ΔTs of about 31-32 ℃ and 27-28 ℃ of lower values at similar levels of ΔTf (~42-43 ℃), which represent a reduction of nearly 14-15% and 24-26%, respectively, of the baseline. The 15 mm and 20 mm fins further dampen ΔTs to approximately 24-25 ℃ and 22-23 ℃, respectively, with similar temperature differences in fluid, which is a total reduction of solid temperatures of about 35-40% of that in the no-fin system.

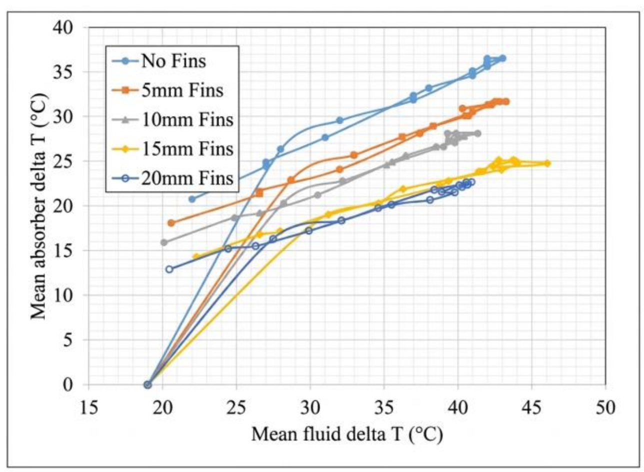

Fig. 8 (d) Character variation of solid and fluid temperature differences

The gradual decrease in ΔTs of a particular ΔTf is a direct confirmation of the augmentation of the effective heat transfer coefficient and fin efficiency. Given the same absorbed heat flux, an increase in (A_{eff}) and (h_{eff}) decreases the temperature forcing potential (T_s- T_f) which is quantitatively captured in Figure 8 (d) by the decrease in ΔTs with the increase in fin height. The efficiency of the fins indicates that the more the fin length (L), the more area, but this is moderated by the conduction resistance in the material of the fin. The fact that the 15 mm and 20 mm curves meet at a higher ΔTf (difference <2 °C past ΔTf ~ 38 °C) indicates a decline in marginal enhancement because of a decrease in fin efficiency and an increase in the axial conduction loss at higher fin heights.

Thermally, top and radiative losses are directly proportional to absorber temperature, and their proportions are proportional. Because the magnitude of losses depends on the absorber temperature, the difference between no-fin and 20 mm-absorber of the same temperature of about 12-14 °C, which reduces the external heat losses, corresponds to the same decrease in net useful heat gain. The fact that all the curves are linear shows that the quasi-steady heat transfer occurs and suggests that the enhancement mechanism is largely a geometric (area and convection augmentation) effect but not a modification of the fluid thermophysical properties [37].

Thus, a progressive increase in fin height also systematically decreases the solid-fluid temperature gradient by as much as 40%, increases the rate of convective heat removal, decreases the temperature of the absorber and reduces external thermal loss. But the marginal gain after 15 mm signifies the beginning of geometric saturation, which is controlled through constraints of fin efficiencies and conduction limits within the extended surfaces.

3.3. Energy Gain and Temperature Distribution

3.3.1. Energy Gain Analysis

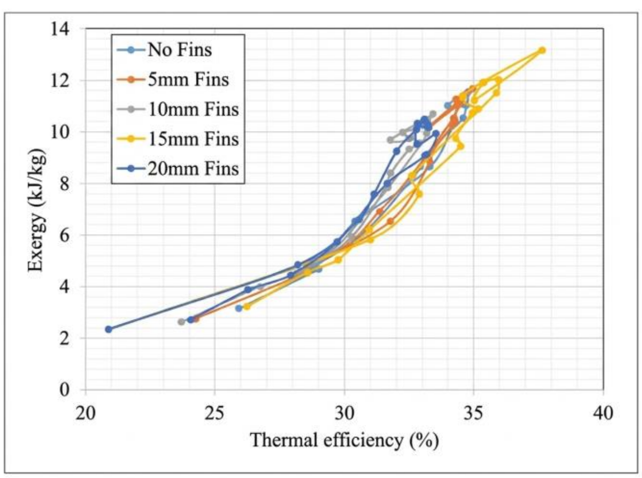

Fig. 9 (a) Energy gain

The response of the thermal efficiency ($\boldsymbol{\eta_{th}}$Specific exergy output (Ex, kJ/kg) to varying transverse fin heights (0-20 mm) as shown in Figure 9 (a), is a quantitative measure of the coupled change in variation between the two variables and is thus a direct measure of the net energy gain through geometric amplification.

A rigorously monotonic exergy increase with thermal efficiency is found in all configurations, which validates the fact that energy gain by enhancing heat transfer through the fins is thermodynamically constructive as opposed to dissipative [38]. The no fins (baseline) design has a thermal efficiency of about 21-33%, with associated exergy gain of about 2.3 to 10.2 kJ/kg. Its efficiency reaches as high as 5 mm fins and has an exergy of approximately 35%, which is almost 11.3 kJ/kg, a specific exergy that is almost 11% greater than the base at the same operating conditions. The 10 mm fin design also increases the exergy to an estimated ~11.6 kJ/kg at an approximate of 34% efficiency, which implies better absorption of heat as the surface area is larger and the coefficient of convective heat transfer is higher. The 15 mm fins exhibit the best performance with a maximum of 13.1 kJ/kg at 38%, and this is equivalent to an approximate increase in exergy by 28-30% above the baseline maximum. This significant increase is proof that augmentation of the surface area is the dominant loss in comparison with both conductive and radiative parasitic losses in this geometrical domain. The 20 mm design, however, exhibits marginal stabilization at a relatively high rate of between ~10.5-10.8 kJ/kg at a relative efficiency of above ~33%, which implies that too high fin height creates an additional conductive resistance and thermal irreversibility, which reduces marginal energy gains even at higher surface area.

3.3.2. Exergy and Entropy Analysis

Exergy analysis is carried out to assess the quality of recovered thermal energy and to analyze the thermodynamic performance of the different absorber configurations investigated. The results showed that the fin height significantly affected the exergy output, with the configuration of 15 mm transverse fins producing the highest exergy output of about 13.1 kJ kg^{-1} as compared to the baseline absorber of 10.2 kJ kg^{-1}, which represents about 28-30% improvement. This improvement in exergy recovery is due to the improvement in conductive heat spreading, the improvement in the absorber–fluid thermal interaction and the increase in useful work potential.

The fin integration increased the temperature uniformity, which resulted in less entropy generation due to the thermal irreversibilities in the system caused by temperature difference and heat-transfer resistance. It was found that the 15 mm configuration had the least thermodynamic irreversibility, the most uniform thermal distribution and the highest exergy utilization. The 20 mm fin configuration had more heat-transfer area, but the lower exergy output indicates a higher conductive resistance and less effective fin. Hence, it can be concluded that the combined exergy and entropy analysis also shows that the 15 mm transverse-fin configuration is the thermodynamic optimal configuration for the effective utilization of solar energy.

The first-law efficiency relation and its exergy analogue are inherently the governors of the observed behaviour of energy gain, and it is obtained by Equation 11,

$$Ex = m[(h - h_0) - T_0(s - s_0)] \quad (11)$$

The fact that the exergy (as represented by the height of the fin) increases progressively to a height of 15 mm confirms that the rise in the rate of exergy gain is inversely proportional to the rate of entropy generation, such that the maximization of the term. $(h - h_0) - T_0(s - s_0)$ is achieved. Past this optimal, more internal temperature gradients and linked irreversibility counteract the marginal increase in absorbed energy, and no more exergy can be increased.

Thus, a 15 mm transverse fin geometry is the best balance between augmented energy absorption and controlled entropy generation, with the most net energy gain and thermodynamic effectiveness of all geometries tested. This, technically, means that the enhancement of performance in such thermal systems is not determined by enlargement of the surface area alone, but by the combination of the augmentation of the heat transfer coefficient, fin efficiency, and rate of entropy generation [39].

3.3.3. Examination of Temporal Variation in mean Fluid Temperature

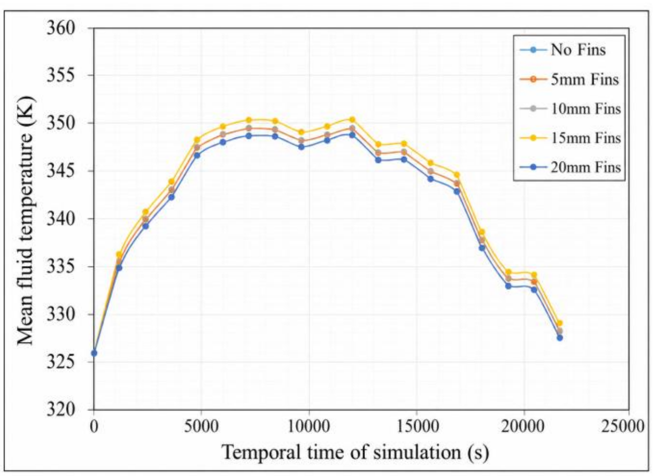

Fig. 9 (b) Temporal variation of mean fluid temperature

Figure 9 (b) shows the temporal change in mean fluid temperature of the base (no fins) and fin-enhanced (5, 10, 15 and 20 mm) configurations during the course of a simulation (= 0-22000 s). The temporal profile has three clear regimes, which are: a fast thermal rise (0-5000 s), a quasi-steady plateau phase (5000-15,000 s), and a late-stage decay phase (15,000 s). At the beginning of the heating, the average fluid temperature rises rapidly with the first 5000 s, and the average heating rate is approximately 4.2-4.6 x 10-3 Ks-1. The presence of the fins will always raise the average fluid temperature over the smooth absorber, and the 15 mm geometry will reach its peak temperature (~350 K) very quickly, and is about 1.5-2.0 K above the no-fin temperature. This improvement can be credited to augmented convectional heat transfer because of augmented effective heat transfer area and augmented mixing of flow, which augments the absorber-to-fluid heat exchange coefficient [22].

The intermediate regime (5000-15,000 s) is the period when the system is close to thermal equilibrium, with the mean temperature of the fluid kept at 348-350 K. The 15 mm and 20 mm fins have a steady benefit of 0.8-1.5 K over the base, which means an efficient conduction of heat spread along the fins and a convective heat transfer to the fluid core. The difference between 15 mm and 20 mm fins is marginal, which means that, when the height of the fin increases, the thermal returns decrease, as the conduction resistance increases with the length of the fin. At about 15,000 s, all the configurations show a monotonic decrease in temperature, to a value of about 328-334 K at 22,000 s. The decay rate of finned systems is slower as it has a higher thermal inertia and better short-term energy storage capacity, with the terminal temperature being almost 1 K lower than the smooth channel.

The brief thermal dynamics of Figure 9 (b) are under fundamental control of the unsteady energy balance of the fluid control volume, which is expressed as in Equation 12.

$$\rho V C_p \frac{dT_m}{dt} = Q_{abs} - mC_p(T_{out} - T_{in}) - UA(T_m - T_a) \quad (12)$$

The net effect of the fin integration on (Q_{abs}) is the net effect of adding to the effective convective surface area and the local heat transfer coefficient (h), which in turn boosts the net term propelling $(\frac{dT_m}{dt})$ at the heating stage. On the other hand, in the decay stage, the loss term $(UA(T_m - T_a))$ dominates the temperature decrease that is observed.

On the whole, the findings verify that the medium fin height, especially 15 mm, is the most effective in transient thermal response as it improves heat transfer through convection but does not pose too much resistance to conduction. The resulting 1-2 K has been found to increase in the peak mean fluid temperature, and this increase indicates enhanced useful energy gain, better thermal stability and higher short-term energy retention, and thus shows that intermediate fin heights offer the best balance between thermal enhancement and geometric efficiency [40].

3.3.4. Temporal Variation of Mean Absorber Temperature

Figure 9 (c) demonstrates the temporary change of the average absorber temperature in the baseline system (no fins) and fin-based systems (5-20 mm) during a period of simulated time (0-22,000 s). Thermal response is three-stage in nature: (i) an initial transient dip at the beginning of the first ~1000 s, (ii) a steady increase in temperatures to the stage of around 8000-12000 s and (iii) a slight decrease at the end of the cycle. Quantitatively, the baseline set-up reaches a peak mean absorber temperature of about 342-343 K, and the addition of fins systematically increases the peak temperature to about 347 K (5 mm), 351 K (10 mm), 354 K (15 mm) and 357 K (20 mm). In this way, the highest increase in the 20 mm fins is associated with a gain of around 14-15 K (~4.2%) as compared to the unfinned condition. This positive monotonic increase proves the fact that the temperature of absorbers increases in a positive manner with the height of the fins.

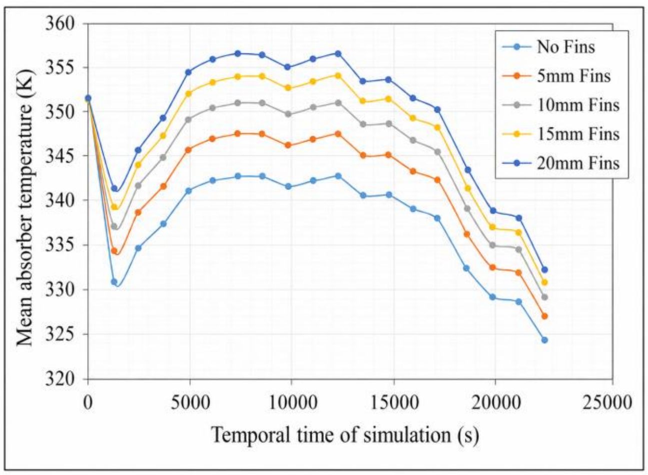

Fig. 9 (c) Temporal variation of mean absorber temperature

The intrinsic principle of thermal amplification is the dynamic energy balance on the absorber surface, which is represented as in Equations 13 & 14.

$$mc_p \frac{dT_m}{dt} = Q_{abs} - Q_{loss} \quad (13)$$

The rate of absorption is provided by

$$Q_{abs} = \alpha I A_{eff} \quad (14)$$

As the convective heat loss term is proportional to surface temperature difference, the temperature increment is moderated but always greater with greater fin heights due to better internal heat distribution and less localized thermal gradients.

The presence of the early-time temperature dip (351 K to 340 K in the 20 mm set-up) shows that the effects of thermal inertia and initial convective losses dominate prior to the establishment of steady irradiative absorption. The quasi-steady behaviour of the temperature plateau (5000-12,000 s) shows that ($\frac{dT_m}{dt}$ = 0) implying ($Q_{abs} - Q_{loss}$). The increased temperature of taller fins at the plateau confirms the enhanced solar energy storage and lowering of entropy generation with the increased conductive spreading of the absorber matrix. The uniform temperature decay in all configurations (with a reduction of the difference between peak and final temperature of the 20 mm system of about 30 K) in the last phase (>15,000 s) indicates a reduction in irradiance or external heat dissipation, but fin-enhanced systems always have a temperature benefit of 5-8 K over the baseline.

This temporal behaviour has an important implication on the performance of thermal systems: the higher the mean temperature of the absorber, the higher the useful heat gain and the instantaneous thermal efficiency [40]. Thus, the 20 mm fin design can be seen to have high thermal energy harvesting capacity during the cycle, which means that geometric enhancement by increasing the height of the fins is effective in enhancing absorber thermal stability as well as peak heat retention during the mid-cycle.

3.3.5. Analysis of Sectioned Temporal Temperature Distributions for all Models

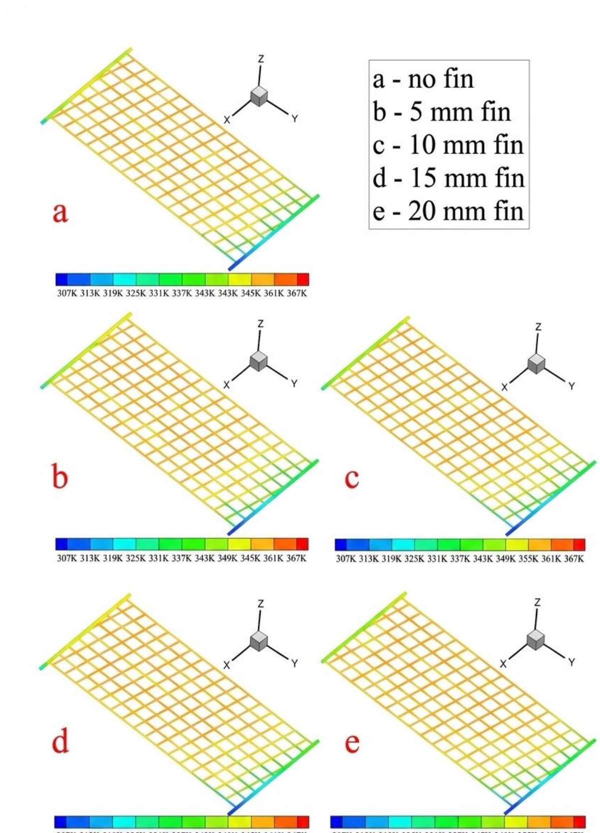

Fig. 10 Sectioned temporal temperature distribution at 10800 Seconds of absorber plate with, (a) No Fins, (b) 5 mm height fins, (c) 10 mm height fins, (d) 15 mm height fins, (e) 20 mm height fins.

The sectional temporal temperature fields at 10800 s (Figure 10 (a)-(e)) are the quasi-steady thermal field of the absorber-fluid domain in the longitudinal fin height of various heights. At this time, the system is near the steady-state, and the temperature field is determined by the conductive heat diffusion in the absorber and convective heat diffusion at the solid-fluid interface. Through the no-fin configuration (Figure 10 (a)), the contours that are sectioned are very non-uniform in terms of thermal properties, with the hottest point being at the center of the absorber because of the low lateral conductivity and low effective heat transfer. The high temperature difference between the solid and fluid phases is a pointer to increased thermal resistance and incomplete heat disposal.

As longitudinal fins (Figures 10 (b) and, (c)) are introduced, the temperature distribution becomes more and more uniform, and the maximum temperature of the absorber is reduced significantly. The fins enhance the effective interfacial area and axial and transverse conduction, and hence reduce thermal gradient and intensity of hotspots.

In 15 mm and 20 mm fin (Figures 10 (d) and, (e)), the additional reduction of the peak temperature is found, but the additional reduction over intermediate fin height is insignificant. It means that there is reduced thermal return with a more conductive path length and lower fin efficiency at higher heights. Though there is an increase in the spatial uniformity of the temperature field, the proportional increase in the heat extraction reduces.

The mean plate temperature is decreased thermodynamically, which reduces heat loss to the surroundings, which is calculated through Equation 15,

$$Q_{loss} = U_L A_p (T_p - T_a) \tag{15}$$

Therefore, fin-assisted designs lower (Tp), reduce thermal losses and enhance collector efficiency. On the whole, the segmented distributions of time substantiate the fact that intermediate fin height (15 mm) offers an optimal compromise between conductive spreading and convective extraction, with maximum thermal performance and without the diminishing returns with excessive fin height.

At 10800 s, the five-layer sectioned temporal temperature distributions (Figures 11 (a) to (e)) obviously determine the effect of longitudinal fin height on internal thermal stratification and absorber-fluid coupling. During this time period, the system gets into the quasi-steady state, during which the absorbed solar energy is mainly compensated by internal conduction and heat extraction through convection. With the no-fin configuration (Figure 11 (a)), there is a strong interlayer temperature gradient, which implies that there is a great internal conduction resistance and that heat is concentrated in the vicinity of the irradiated surface. The high ratio of maximum to minimum sectional temperature difference confirms that lateral heat diffusion to the risers is inefficient, resulting in a rise in peak absorber temperatures and an increase in thermal non-uniformity. These large spatial gradients suggest that more entropy is generated in the solid domain and the possible concentration of thermal stresses in the long-run.

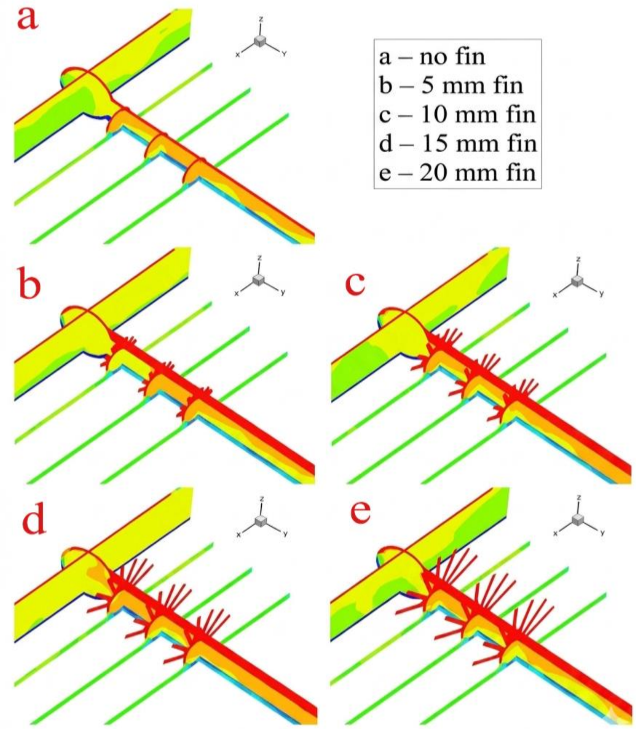

Fig. 11 Five-layer sectioned temporal temperature distribution at 10800 Seconds of absorber plate with, (a) No Fins, (b) 5 mm height fins, (c) 10 mm height fins, (d) 15 mm height fins, (e) 20 mm height fins.

The transient heat conduction, as given in equation 16 with internal heat generation, is referred to as the governing mechanism.

$$\rho_s c_{p,s} \frac{\partial T}{\partial t} = k_s \nabla^2 T + q_{abs} \tag{16}$$

When there is no fin, the limited conductive pathways allow the diffusion term ($k_s \nabla^2 T$) to maintain a higher sectional gradient.

There was a systematic decrease in the interlayer temperature differences and increased uniformity of the sectional temperature profiles as fin height was increased progressively by 5 mm to 20 mm (Figures 11 (b)-(e)). The fins maximize the effective conducting paths and minimise thermal conductivities between the absorber surface and the riser region, and enhance the diffusion term in the solid energy equation. At the same time, the effective heat transfer area is enhanced, enhancing the convective heat extraction. The growth in (A_{eff}) directly boosts useful heat transfer, helps moderate the peaks in absorber temperatures and inhibits sectional thermal stratification.

With the 20 mm fin arrangement (Figure 11 (e)), the near-uniform five-layer distribution at 10800 s ensures high values of low internal thermal resistance and high conduction-convection synergy. All of these fin configurations suggest that a higher fin height leads to increased sectional thermal homogenization, smaller peak thermal accumulation, less entropy generation relating to large temperature gradients, better absorber-fluid thermal interaction, and, therefore, improved thermal efficiency and structural reliability in sustained operating conditions.

3.4. CFD-based Thermohydraulic Optimization

The Thermohydraulic Performance Index (THPI) was used as an overall performance metric to account for both thermal benefit and hydraulic loss in order to determine the best configuration of transverse fins, and is defined as in equation (17):

$$THPI = \frac{\eta/\eta_0}{\Delta P/\Delta P_0} \tag{17}$$

Where: η = thermal efficiency of finned configuration; ΔP = pressure drop of finned configuration; η_0 = thermal efficiency of baseline absorber plate; ΔP_0 = pressure drop of baseline absorber plate; THPI = Thermohydraulic Performance Index

A CFD-based thermohydraulic optimization was carried out to determine the best transverse-fin configuration considering both thermal enhancement and hydraulic penalty simultaneously through a Thermohydraulic Performance Index (THPI). It was found that an increase in fin height resulted in increased heat-transfer performance due to better conductive heat spreading and absorber–fluid thermal interaction, but also in higher hydraulic resistance and pressure-drop penalties. The configuration with transverse fins of 15 mm was found to be the most promising in terms of thermal efficiency improvement and hydraulic performance among the configurations investigated. The 20 mm configuration provided more area, but the resulting extra thermal gains were small compared to the extra pressure drop, leading to a lower thermohydraulic effectiveness. Thus, the optimization validates the 15 mm fin height as the optimum design for the investigated geometry of solar water heater and operating conditions, and it proves the effectiveness of CFD as a design optimization tool for fin-enhanced solar water heater absorber plate.

3.5. Literature Contextualization and Comparison

The results of the present study are in line with the recent studies on the enhancement techniques of solar collectors reported in the literature. Alternative enhancement techniques such as wavy fins, pin fins, louvered fins, corrugated absorbers, rib roughened surfaces, turbulence promoters, and PCM-assisted collectors have shown an increase in heat-transfer performance by increasing surface area, flow mixing, and boundary-layer disruption. But these methods often come with higher pressure drop penalties, fabrication complexity and/or added system costs. The optimized 15 mm transverse-fin configuration, on the other hand, resulted in better temperature uniformity, useful heat gain, thermal efficiency, and exergy performance with acceptable hydraulic characteristics and manufacturing simplicity. The findings also corroborate recent research that geometric optimization is an important aspect of the trade-off between heat-transfer enhancement and hydraulic losses. Thus, the present study contributes to the ongoing research on passive enhancement of heat transfer by developing a thermohydraulically optimized design of the transverse-fin that can be manufactured and implemented on a large scale in a practical manner while maintaining high thermal performance and hydraulic efficiency.

3.6. Environmental, Economic, and Scalability Implications

The equation (18) was used to calculate the thermal efficiency of the collector, which is defined as the ratio of the useful heat gain to the incident solar energy that is effectively transferred to the working fluid. The higher the thermal efficiency, the more solar energy that is used, the more economic the system will be, and the less auxiliary energy will be needed, which means a lower impact on the environment. In addition to the improved thermohydraulic performance, the optimized 15 mm transverse-fin configuration delivers environmental, economic and practical implementation benefits. The heat-transfer effectiveness was improved, and the useful energy utilization was increased, and the overall heat losses were reduced by about 34–38% as compared to the unfinned absorber, thereby reducing the need for conventional water-heating systems and the associated greenhouse-gas emissions.

$$\eta_{th} = \frac{Q_u}{IA_c} \tag{18}$$

Where: Qu = Useful heat gain (W) ; I = Incident solar irradiance (W m^{-2}); Ac = Effective collector area (m^2); ηth = Thermal efficiency of the solar collector (-).

Transverse fins are passive enhancements, which means that they do not add any extra power consumption or auxiliary parts. The fin integration was found to increase material use, but the 15 mm configuration was found to provide the greatest thermal benefit, while additional increases in fin height resulted in marginal increases in performance. Moreover, the proposed design can be easily fabricated using the existing flat-plate collector fabrication process, which shows the economic feasibility and scalability for large-scale solar water-heating applications.

3.7. Long-Term Performance and Durability Considerations

The temperature uniformity and thermal stability of collectors are key factors in collector durability. Transverse fins were found to enhance the heat spreading effect and minimize the temperature accumulation, with the 15 mm configuration showing the most desirable temperature uniformity, thermal efficiency, exergy utilization and reduction of heat loss. The reduction of heat losses by about 34–38% shows that there are lower thermal gradients and thermally induced stresses, which can reduce localized overheating and material degradation during extended periods of operation. The absorber proposed here is of a transverse-fin design that can be easily incorporated into the current building-scale solar water-heating systems with limited changes in the collector design and production. The optimized 15 mm configuration is especially recommended for residential, commercial and institutional hot-water applications where the enhanced thermal performance can help to utilize more solar energy and lower auxiliary energy requirements.

4. Conclusion

This paper numerically examined the thermohydraulic characteristics of solar water heater absorbers with transverse plate fins of different heights (0 to 20 mm) in a transient conjugate heat transfer CFD model, which has the following consolidated findings:

- Thermal efficiency exhibits a non-monotonic variation with fin height, although the increase in surface area is approximately 150 percent, with the 15 mm set-up being recognized as optimal, and giving 5 percent higher efficiency than the baseline, with quasi steady values of 34-38 percent.
- Fin heights of (5 & 10 mm) decrease efficiency by ~3.2% & ~7% because of more conduction resistance and less fin effectiveness, and with the 20 mm height, the combined effect of conduction, convective-radiative losses and increased fin inefficiency leads to a reduction by ~10% compared to the height of 15 mm peak.
- The transient thermal performance includes three different regimes: intense heating (0-3000 s), quasi-steady plateau (4000-17,000 s), and cooling (>17,000 s), with the 15 mm fins responding the quickest and most stable to the new system, with peak performance (~38%) existing near 11,000 s.
- The temperature of the absorbers is enhanced by fin height, whereby 20 mm fins enhance temperatures by approximately 22-23 K (~7% above baseline) compared to the base temperature, and 15 mm configuration reaches an absorber temperature of 354 K and fluid temperature of 350 K (~2.0 K above base temperature). Though the 20 mm fins get the highest absorber temperature ~357 K, their efficiency is lower ~33%; subsequently, they have higher thermal resistance and fin inefficiency.
- The solid-fluid temperature differences are reduced by up to 40% with the addition of fins (especially 15-20 mm), suggesting a higher level of convective coupling and a lower level of thermal loss. The heat loss is decreased with increasing fin heights, especially the 20 mm fin configuration, which provided the maximum reduction of ~37%, yet this configuration does not yield the maximum efficiency because of internal conduction penalties.
- Maximum exergy output is reached with 15 mm fins (approximately 13.1 kJ/kg, 28 times higher than the baseline), but lower values are found with 20 mm fins (10.5-10.8 kJ/kg) at approximately 33% efficiency, which is an indication of higher irreversibility.
- Sectional temperature distributions (~10,800 s) validate optimal thermal uniformity with fin height, 15 mm offers the optimal condition between conductive spreading and convective extraction, and 20 mm only offers a marginal additional advantage. The hydraulic penalties (pressure drop and power of pumping) increase with the height of the fin and decrease the net performance beyond 15 mm, and thus 15 mm is found to be the optimal substitution.
- Overall, the 15 mm fin design offers the balanced thermogeometric solution, with the highest thermal efficiency (38%), highest absorber temperature (354 K), maximum fluid temperature (350 K), and exergy output (maximum energy of 13.1 kJ/kg), and least temperature gradients (reduction of temperature by 40%) and stable operation at 11,000 s.

Future Scope

In the future, the use of parametric optimization, multi-objective optimization algorithms, and machine-learning-assisted design methodologies in conjunction with the CFD-generated datasets could be used to predict and optimize simultaneously the thermal efficiency, exergy performance, and hydraulic characteristics in a much wider range of operating conditions.

Funding

This research received no specific grant from any funding agency in the public, commercial, or not-for-profit sectors.

Conflicts of Interest

The authors declare that there is no conflict of interest.

References

[1] Amal Herez et al., "Solar Water Heating: Comprehensive Review, Critical Analysis and Case Study," *International Journal of Thermofluids*, vol. 20, pp. 1-27, 2023. [CrossRef] [Google Scholar] [Publisher Link]

[2] Mehdi Ahmadi Jirdehi, Mohammad Shaterabadi, and Atif Iqbal, "Enhancement of the Solar Water Heater Thermodynamic Performance by Utilizing Solar Panels under Diverse Scenarios: Comprehensive Outlook," *International Communications in Heat and Mass Transfer*, vol. 163, 2025. [CrossRef] [Google Scholar] [Publisher Link]

[3] Walid Zaafouri et al., “Experimental Study of a New Vertical Solar Water Heater Design under Varied Seasonal Weather Conditions in Gabes City,” *Results in Engineering*, vol. 28, pp. 1-13, 2025. [CrossRef] [Google Scholar] [Publisher Link]

[4] Mohammad Zaboli et al., “Thermohydraulic and Data-Driven–Probabilistic Modelling of a Turbulator-Enhanced Hybrid Solar–Gas Water Heater for Global Technoeconomic and Environmental Performance Prediction,” *Energy Conversion and Management*, vol. 353, 2026. [CrossRef] [Google Scholar] [Publisher Link]

[5] Leilei Fan, and Wuyi Wan, “Numerical Analysis of Convective Flows in Solar Water Heating Systems: Toward Large-Scale Implementation,” *Applied Thermal Engineering*, vol. 290, 2026. [CrossRef] [Google Scholar] [Publisher Link]

[6] Shayan Mohammaddini et al., “Techno-Economic Simulation of Solar Flat Plate Collector Systems for Building Hot Water Demand Supply,” *Energy*, vol. 338, 2025. [CrossRef] [Google Scholar] [Publisher Link]

[7] Md. Shamiul Basar Himel et al., “Experimental Performance Investigation on the Effect of Step Change in Absorber Plate Thickness of Flat Plate Solar Collector,” *Next Sustainability*, vol. 6, pp. 1-13, 2025. [CrossRef] [Google Scholar] [Publisher Link]

[8] Ali Rmaidh Badr et al., “Enhancing the Efficiency of Solar Water Heaters with Phase Change Materials: Numerical Assessment,” *International Communications in Heat and Mass Transfer*, vol. 166, 2025. [CrossRef] [Google Scholar] [Publisher Link]

[9] Himsar Ambarita et al., “Numerical Simulation of Heat Transfer of an Absorber with Fin of a Flat-Plate Type Solar Collector,” *IOP Conference Series: Materials Science and Engineering: 2nd Nommensen International Conference on Technology and Engineering*, Medan, Indonesia, vol. 420, pp. 1-8, 2018. [CrossRef] [Google Scholar] [Publisher Link]

[10] M. D. Sagar et al., “A Comprehensive Review on Geometric Variations in Fin Configurations: Experimental and Mathematical Studies,” *Archives of Computational Methods in Engineering*, vol. 33, pp. 6451-6500, 2026. [CrossRef] [Google Scholar] [Publisher Link]

[11] Moataz M. Abdel-Aziz et al., “Thermal Performance Enhancement of Solar Collectors through Optimization of Outlet Temperature,” *Environmental Progress & Sustainable Energy*, vol. 45, no. 1, 2026. [CrossRef] [Google Scholar] [Publisher Link]

[12] Rahul Khatri et al., “Effects of Surface Geometries and Fin Modifications on the Thermal Performance of Solar Air Heaters: A Review,” *Advances in Fluid and Thermal Engineering*, pp. 409-421, 2021. [CrossRef] [Google Scholar] [Publisher Link]

[13] E. Flilihi et al., “Effect of Absorber Design on Convective Heat Transfer in a Flat Plate Solar Collector: A CFD Modeling,” *Frontiers in Heat and Mass Transfer*, vol. 18, pp. 1-6, 2022. [CrossRef] [Google Scholar] [Publisher Link]

[14] S. Madhankumar et al., “Comparative Energy, Environmental and Economic Analysis of Solar Air Heaters with Corrugated and Sinusoidal Absorber Plates with Thermal Energy Storage,” *Applied Thermal Engineering*, vol. 279, 2025. [CrossRef] [Google Scholar] [Publisher Link]

[15] Nugroho Agung Pambudi, Iksan Riva Nanda, and Andi Dwi Saputro, “The Energy Efficiency of a Modified v-Corrugated Zinc Collector on the Performance of Solar Water Heater (SWH),” *Results in Engineering*, vol. 18, pp. 1-12, 2023. [CrossRef] [Google Scholar] [Publisher Link]

[16] Dilbag Singh Mondloe, Harish Kumar Ghritlahre, and Gajendra Kumar Agrawal, “The Evaluation and Development of Correlation for Heat Transfer and Fluid Flow Characteristics in Solar Air Heaters using Gapped Transverse wire Ribs-An Experimental Study,” *International Journal of Thermal Sciences*, vol. 218, 2025. [CrossRef] [Google Scholar] [Publisher Link]

[17] Dilbag Singh Mondloe, Harish Kumar Ghritlahre, and Gajendra Kumar Agrawal, “Thermal and Thermohydraulic Performances of Solar Air Heater using Transverse Wire Rib Roughness with Various Gaps- An Experimental Study,” *Solar Energy*, vol. 300, 2025. [CrossRef] [Google Scholar] [Publisher Link]

[18] N. Gunasekaran et al., “Investigation on ETC Solar Water Heater using Twisted Tape Inserts,” *Materials Today: Proceedings*, vol. 47, pp. 5011-5016, 2021. [CrossRef] [Google Scholar] [Publisher Link]

[19] Channaveerayya Mathapati et al., “Performance Analysis of V-Trough Solar Water Heater using Curve Shaped Riser Tubes with Coil Inserts,” *Thermal Advances*, vol. 6, pp. 1-8, 2026. [CrossRef] [Google Scholar] [Publisher Link]

[20] Hadi Samimi-Akhijahani et al., “Eco-Efficient Solar Water Desalination System: Integrating Phase Change Materials, Geothermal and Spraying Units,” *Applied Thermal Engineering*, vol. 286, 2026. [CrossRef] [Google Scholar] [Publisher Link]

[21] Mohamed Bechir Ben Hamida et al., “Intelligent Design Framework for Finned Solar Air Heaters: A Synergy between PSO/GA-Tuned MLPNN and Multi-Objective Crystal Structure Algorithm (MOCryStAl),” *International Communications in Heat and Mass Transfer*, vol. 169, 2025. [CrossRef] [Google Scholar] [Publisher Link]

[22] Parag Jyoti Bezbaruah, Rajat Subhra Das, and Bikash Kumar Sarkar, “Solar Air Heater with Finned Absorber Plate and Helical Flow Path: A CFD Analysis,” *Applied Solar Energy*, vol. 56, pp. 35-41, 2020. [CrossRef] [Google Scholar] [Publisher Link]

[23] G. Vivek et al., “Optimization and Simulation of a Solar Flat Plate Collector Using Response Surface Methodology and Computational Fluid Dynamics,” *International Journal of Engineering Trends and Technology*, vol. 74, no. 2, pp. 19-41, 2026. [CrossRef] [Publisher Link] duplicate

[24] Ali Tavakoli et al., “Physics-based Modelling and Data-Driven Optimisation of a Latent Heat Thermal Energy Storage System with Corrugated Fins,” *Renewable Energy*, vol. 217, pp. 1-13, 2023. [CrossRef] [Google Scholar] [Publisher Link]

[25] Ping Liu et al., “Heat Transfer Enhancement of Microchannel Heat Sink Using Sine Curve Fins,” *Journal of Thermophysics and Heat Transfer*, vol. 38, no. 3, 2024. [CrossRef] [Google Scholar] [Publisher Link]

[26] Zia Ud Din et al., "Investigation of Heat Transfer from Convective and Radiative Stretching/Shrinking Rectangular Fins," *Mathematical Problems in Engineering*, vol. 2022, pp. 1-10, 2022. [CrossRef] [Google Scholar] [Publisher Link]

[27] Binit Kumar et al., "Numerical Analysis of Absorber Tube Shapes in PCM-Integrated Parabolic Trough Solar Collectors" *Case Studies in Thermal Engineering*, vol. 66, pp. 1-15, 2025. [CrossRef] [Google Scholar] [Publisher Link]

[28] Peng Zhao et al., "Ultrahigh Thermal Robustness of High-Entropy Spectrally Selective Absorbers for Next-Generation Concentrated Solar Power System," *Advanced Functional Materials*, vol. 34, no. 52, 2024. [CrossRef] [Google Scholar] [Publisher Link]

[29] W. Haw, C. S. Oon, and E. V. Lau, "Analysis of Hydrodynamics and Thermal–Hydraulic Performance of Twisted Angle Fins within an Annular Conduit," *Journal of Thermal Analysis and Calorimetry*, vol. 150, pp. 377-394, 2024. [CrossRef] [Google Scholar] [Publisher Link]

[30] Naveen Sharma, Andallib Tariq, and Manish Mishra, "Experimental Investigation of Heat Transfer Enhancement in Rectangular Duct with Pentagonal Ribs," *Heat Transfer Engineering*, vol. 40, no. 1-2, pp. 147-165, 2019. [CrossRef] [Google Scholar] [Publisher Link]

[31] Zhan Liu et al., "Effect of Phase Change Heat Storage Tank with Gradient Fin Structure on Solar Energy Storage: A Numerical Study," *International Journal of Heat and Mass Transfer*, vol. 215, pp. 1-14, 2023. [CrossRef] [Google Scholar] [Publisher Link]

[32] G. Sowmya et al., "Significance of Convection and Internal Heat Generation on the Thermal Distribution of a Porous Dovetail Fin with Radiative Heat Transfer by Spectral Collocation Method," *Micromachines*, vol. 13, no. 8, pp. 1-20, 2022. [CrossRef] [Google Scholar] [Publisher Link]

[33] Florent Bunjaku, Kastriot Buza, and Risto V. Filkoski, "Comparative Analysis of Thermal Performance and Geometric Characteristics of Tubes with Rectangular and Triangular Fins," *Processes*, vol. 13, no. 10, pp. 1-17, 2025. [CrossRef] [Google Scholar] [Publisher Link]

[34] Ran Ju et al., "Convective Thermal Metamaterials: Exploring High-Efficiency, Directional, and Wave-Like Heat Transfer, Directional, and Wave-Like Heat Transfer," *Advanced Materials*, vol. 35, no. 23, pp. 1-17, 2023. [CrossRef] [Google Scholar] [Publisher Link]

[35] Noushin Azimy, Mohammad Reza Saffarian, and Aminreza Noghrehabadi, "Thermal Performance Analysis of a Flat-Plate Solar Heater with Zigzag-Shaped Pipe Using Fly Ash-Cu Hybrid Nanofluid: CFD Approach," *Environmental Science and Pollution Research*, vol. 31, no. 12, pp. 18100-18118, 2022. [CrossRef] [Google Scholar] [Publisher Link]

[36] Haiyi Sun et al., "Molecular Dynamics Study of Convective Heat Transfer Mechanism in a Nano Heat Exchanger," *RSC Advances*, vol. 10, no. 39, pp. 23097-231074, 2020. [CrossRef] [Google Scholar] [Publisher Link]

[37] Yuting Jia et al., "Heat Transfer and Fluid Flow Characteristics of Microchannel with Oval-Shaped Micro Pin Fins," *Entropy*, vol. 23, no. 11, pp. 1-17, 2021. [CrossRef] [Google Scholar] [Publisher Link]

[38] Abdolvahab Ravanji et al., "Critical Review on Thermohydraulic Performance Enhancement in Channel Flows: A Comparative Study of Pin Fins," *Renewable and Sustainable Energy Reviews*, vol. 188, pp. 1-20, 2023. [CrossRef] [Google Scholar] [Publisher Link]

[39] Lei Zhang et al., "Numerical Study of Fin-and-Tube Heat Exchanger in Low-Pressure Environment: Air-Side Heat Transfer and Frictional Performance, Entropy Generation Analysis, and Model Development," *Entropy*, vol. 24, no. 7, pp. 1-19, 2022. [CrossRef] [Google Scholar] [Publisher Link]

[40] Nishant Modi, Xiaolin Wang, Michael Negnevitsky, "Experimental Investigation of the Effects of Inclination, Fin Height, and Perforation on the Thermal Performance of a Longitudinal Finned Latent Heat Thermal Energy Storage," *Energy*, vol. 274, pp. 1-19, 2023. [CrossRef] [Google Scholar] [Publisher Link]